SCIENTIFIC REPORTS
nature research

OPEN

Defect processes in F and Cl doped anatase TiO_2

Petros-Panagis Filippatos[1,2], Nikolaos Kelaidis[2,3], Maria Vasilopoulou[1*], Dimitris Davazoglou[1], Nektarios N. Lathiotakis[3] & Alexander Chroneos[2,4*]

Titanium dioxide represents one of the most widely studied transition metal oxides due to its high chemical stability, non-toxicity, abundance, electron transport capability in many classes of optoelectronic devices and excellent photocatalytic properties. Nevertheless, the wide bang gap of pristine oxide reduces its electron transport ability and photocatalytic activity. Doping with halides and other elements has been proven an efficient defect engineering strategy in order to reduce the band gap and maximize the photocatalytic activity. In the present study, we apply Density Functional Theory to investigate the influence of fluorine and chlorine doping on the electronic properties of TiO_2. Furthermore, we present a complete investigation of spin polarized density functional theory of the (001) surface doped with F and Cl in order to elaborate changes in the electronic structure and compare them with the bulk TiO_2.

Transition metal oxides such as titanium dioxide (TiO_2) are considered as an extremely important class of materials due to their intense catalytic activity, superior chemical stability, long life cycle and high electrical conductivity[1–10]. Particularly, anatase TiO_2 has been extensively studied because of its abundance and non-toxicity, high photocatalytic activity and responseto visible light arising from high its absorption coefficient and reflectivity[1–10]. Moreover, it represents the work-horse photoanode material in dye-sensitized solar cells (DSSCs)[11–16], whereas recently has been widely applied as the device electron transport material in both organic-inorganic halide perovskite (PSC) and organic solar (OSC) cells[17–25]. Nevertheless, TiO_2 exhibits a wide band gap of around 3.2 eV[26,27] that limits its absorption in the visible and, especially, in the near infrared (NIR) region[7]. A common way to reduce the band gap of TiO_2 is through doping with appropriate elements which has also significant impact on its electronic structure. A vast variety of literature reports previously demonstrated that by doping TiO_2 with nitrogen (N), halogens such as fluorine (F) and chlorine (Cl), or several transition metal ions such as zinc (Zn) or nickel (Ni), significant changes in its electronic structure are observed[28–34]. Particularly, the formation of mid gap states resulting in a band gap reduction was evident. For instance, when titanium dioxide is doped with Ni the band gap decreases to 2.57 eV,[33] whereas when it is doped with Cl mid gap states are formed and the band gap decreases to 3 eV[31]. Progress on the photocatalytic performance and heterogeneous catalysis of TiO_2 and other oxides such as ZnO has also been accomplished by the introduction of oxygen vacancies[35,36] combined with metallic doping.

Focusing on other defect related projects regarding the TiO_2 and its application to photocatalysis, it is seen that TiO_2 has a fast recombination of the conduction band electrons and valence band holes and as a result it is not a satisfactory photocatalytic for organic degradation. In order to solve that problem as well as to reduce the large band gap, it is seen in the literature that many doped models of TiO_2 can have improved photocatalysis. For example, N doped TiO_2[37] and Nb doped TiO_2[38] is reported to have better photocatalytic properties than pure TiO_2.

Although a profound band gap reduction can be beneficial to the material's photocatalytic activity as it results in higher absorption of visible light, it might create mid gap states that usually act as charge traps hence having a negative impact on the performance of organic and perovskite solar cells utilizing TiO_2 exclusively as electron transport/extraction material[39]. In those cases the photocatalytic ability of TiO_2 should be suppressed as it degrades its interface with organic/perovskite semiconductor. The formation of mid gap states upon doping

[1]Institute of Nanoscience and Nanotechnology (INN), National Center for Scientific Research Demokritos, 15310, AgiaParaskevi, Athens, Greece. [2]Faculty of Engineering, Environment and Computing, Coventry University, Priory Street, Coventry, CV1 5FB, United Kingdom. [3]Theoretical and Physical Chemistry Institute, National Hellenic Research Foundation, Vass. Constantinou 48, GR-11635, Athens, Greece. [4]Department of Materials, Imperial College, London, SW7 2AZ, United Kingdom. *email: m.vasilopoulou@inn.demokritos.gr; alexander.chroneos@imperial.ac.uk

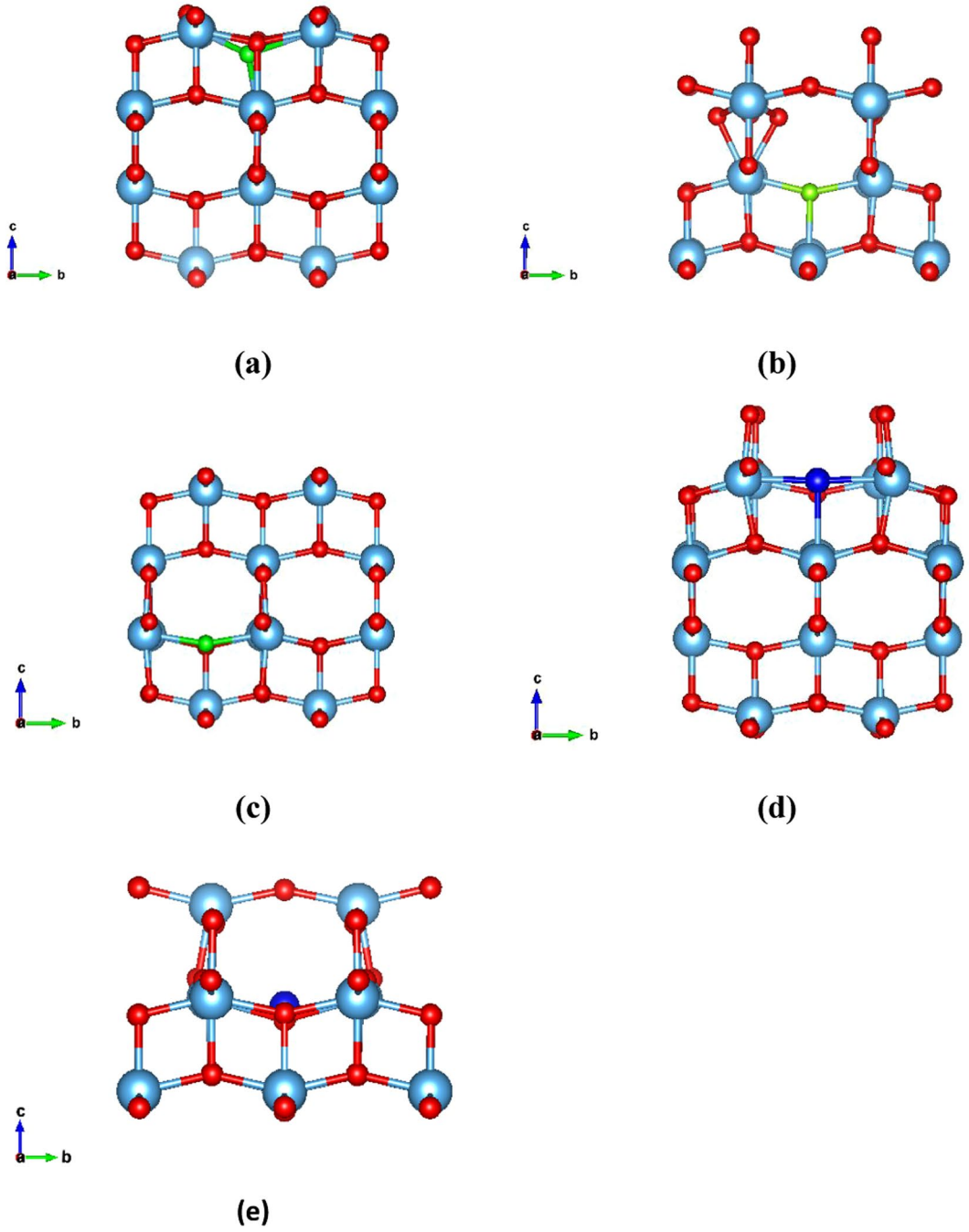

Figure 1. (**a**) The minimum energy structure of fluorine interstitial doped anatase TiO_2, (**b**) The minimum energy structure of the F doped bulk TiO_2 where F occupies an oxygen site, (**c**) The minimum energy structure of the substitutional F on the bulk anatase TiO_2, (**d**) The minimum energy structure of the chlorine substitutional doped bulkanatase TiO_2, (**e**) The minimum energy structure of the chlorine interstitial doped bulk anatase TiO_2.

of TiO_2 is therefore undesired in OSCs and PSCs. In the present study, fluorine and chlorine doping of the bulk and surface TiO_2 is studied via Density Functional Theory (DFT) in order to examine the electrical structure before and after doping with F and Cl and investigate the potential improvement in the photocatalytic activity of the TiO_2. Moreover we investigated many different defect sites for the F and Cl in the bulk system and we also calculated for the first time the interstitial sites and the changes in electrical properties of the (001) TiO_2 surface after the F and Cl doping. Total density of states (DOS) and partial DOS (PDOS) of the energetically minimum sites of the defects are considered in order for the electrical structure changes to be fully understood. A band gap reduction is evident in both cases. Moreover, the formation of mid gap states in all cases is also predicted. Such states are highly beneficial for the photocatalytic applications of TiO_2 though they can be detrimental for

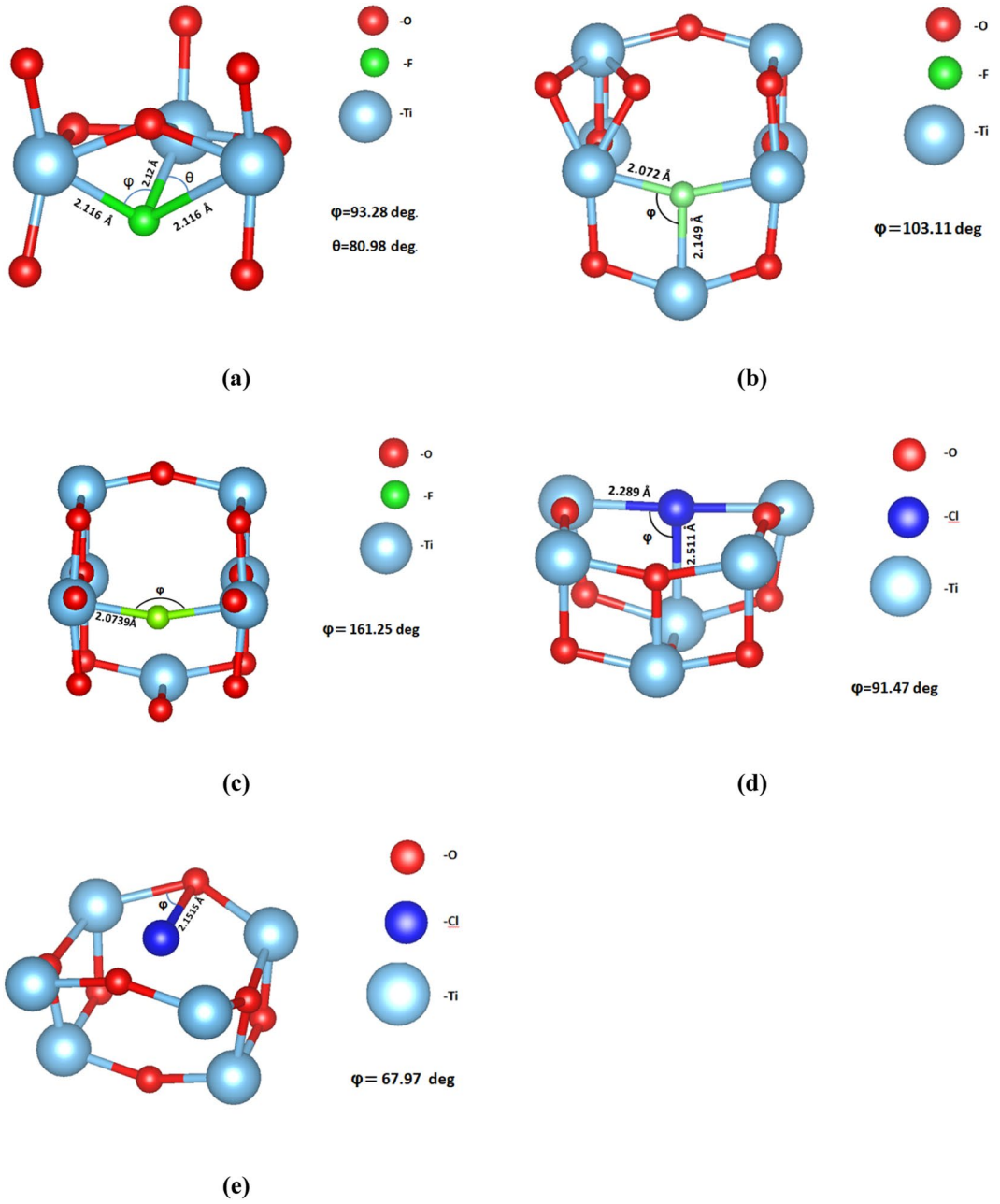

Figure 2. (**a**) The fluorine interstitial in the bulk TiO_2, (**b**) The fluorine interstitial in the bulk TiO_2 when the oxygen atom is displaced, (**c**) The fluorine substitutional in the bulk TiO_2, (**d**) The Chlorine substitutional in the bulk TiO_2, (**e**) The Chlorine interstitial in the bulk TiO_2.

OSCs and PSCs performance as they constitute trap sites for the photogenerated charge carriers thus significantly reducing the device photocurrent.

Results and Discussion

Bulk anatase TiO_2. There are three polymorphs of TiO_2 (rutile, anatase and brookite) with the anatase being the prevalent choice for photovoltaic applications as it has superior photocatalytic properties[40]. The crystal structure for the anatase is tetragonal with space group I4/amd and its experimental structural parameters calculated from neutron diffraction are a = 3.782 Å, b = 3.782 Å and c = 9.502 Å[41]. Our theoretically calculated lattice parameters of the anatase are a = 3.804 Å, b = 3.804 Å and c = 9.729 Å which also agree with other theoretical results[42,43]. The percentage of our dopants was 1 dopant atom per 109 atoms of TiO_2 (0.91% doping). In the surface system we calculated 1 dopant atom per 96 atoms of TiO_2 (1.04% additional doping). As regards the density of F and Cl atoms in the bulk systems, we calculated that for the F interstitial we have a density of 7.863 10^{20} cm^{-3}, for the F substitutional we have a density of 7.872·10^{20} cm^{-3} and lastly for the Cl interstitial and Cl substitutional we have a density of 7.825·10^{20} cm^{-3} and 7.829 10^{20} cm^{-3} respectively. On the other hand, for the surfaces, we calculated

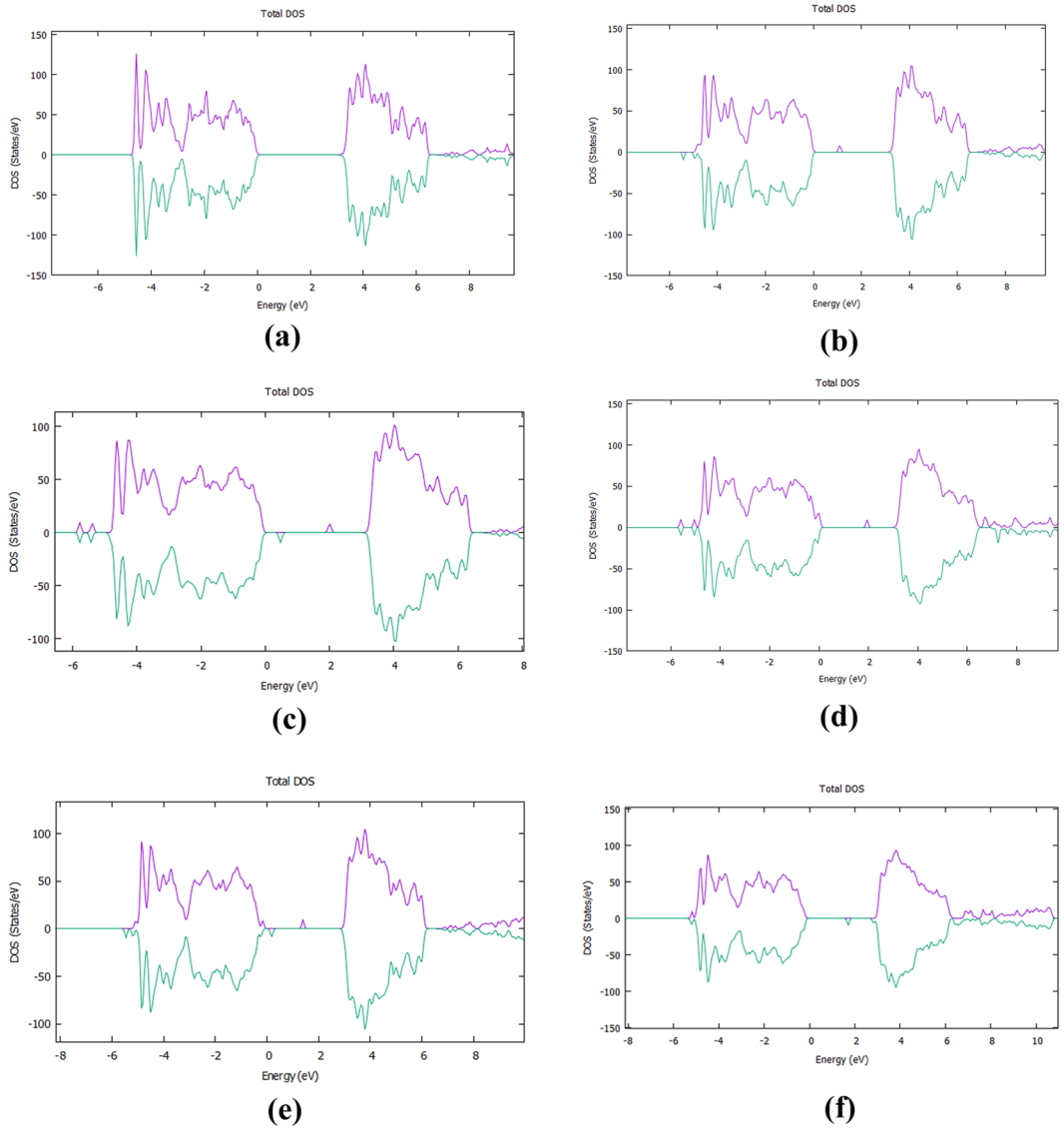

Figure 3. (**a**) DOS of the undoped bulk anatase TiO_2, (**b**) DOS of interstitially F - doped TiO_2 (**c**) DOS of F:TiO_2 with F substituting an Oxygen site and displacing it to an interstitial site. (**d**) DOS of the F:TiO_2 when F is a substitution to O, (**e**) The Density of States graph of the Cl-Doped TiO_2 with Cl as an interstitial, (**f**) The Density of States graph of the Cl:TiO_2 when Cl is a substitution to O.

a density of $4.451 \cdot 10^{20}$ cm^{-3} for the F interstitial and $4.423 \cdot 10^{20}$ cm^{-3} for the Cl interstitial. According to our DFT calculations, the F atom is stable either as an oxygen substitutional defect or an interstitial defect in the bulk TiO_2 system. We found that in the case of interstitial, the fluorine atom is located at a distance of 1.983 Å from the nearest oxygen atom (see Figs. 1a and 2a) in agreement with previous studies[33]. Examining thoroughly the various defect formations, we concluded that the minimum energy configuration is when fluorine occupies an oxygen site displacing the oxygen to an interstitial site, as seen in Figs. 1b and 2b. Moreover, the simple substitution of an O atom with F has also been examined (Figs. 1c, 2c). Concerning Cl atom doping of bulk TiO_2, we show that the Cl can either substitute an oxygen atom or relax in a substitutional position, at a distance of 2.15 Å from the nearest oxygen atom (Figs. 1d,e and 2d,e).

For each supercell, we calculated the DOS (Fig. 3(a)–(f)) and, in Fig. 3a, the total DOS of the pure TiO_2 is shown as a reference. Our calculations were performed with DFT + U model with the Hubbard-U parameter equal to 8.2 eV[33,34]. We calculated the band gap at 3.14 eV, in agreement with previous theoretical studies[33,34,44], which show a band gap narrowing from 3 to 3.16 eV and close to the experimental value of 3.2 eV.

As we show in Fig. 3b, the F interstitial in the bulk TiO_2 gives rise to a small peak inside the band gap at approximately 0.98 eV above the valence band (VB) and it also decreases the band gap to 3.04 eV. When an oxygen atom is replaced by a fluorine, the mid-gap impurity band is shifted towards the conduction band (Fig. 3d). Figure 4(a)–(d) represents the PDOS of doped and undoped bulk TiO_2. In order to fully understand the emergence of the mid-gap peak in the case of the F interstitial, we calculated the partial DOS which is shown in Fig. 4a. Figure 5(a)–(f) examines in more detail the PDOS and the orbital contribution to the mid gap rise. There, one can

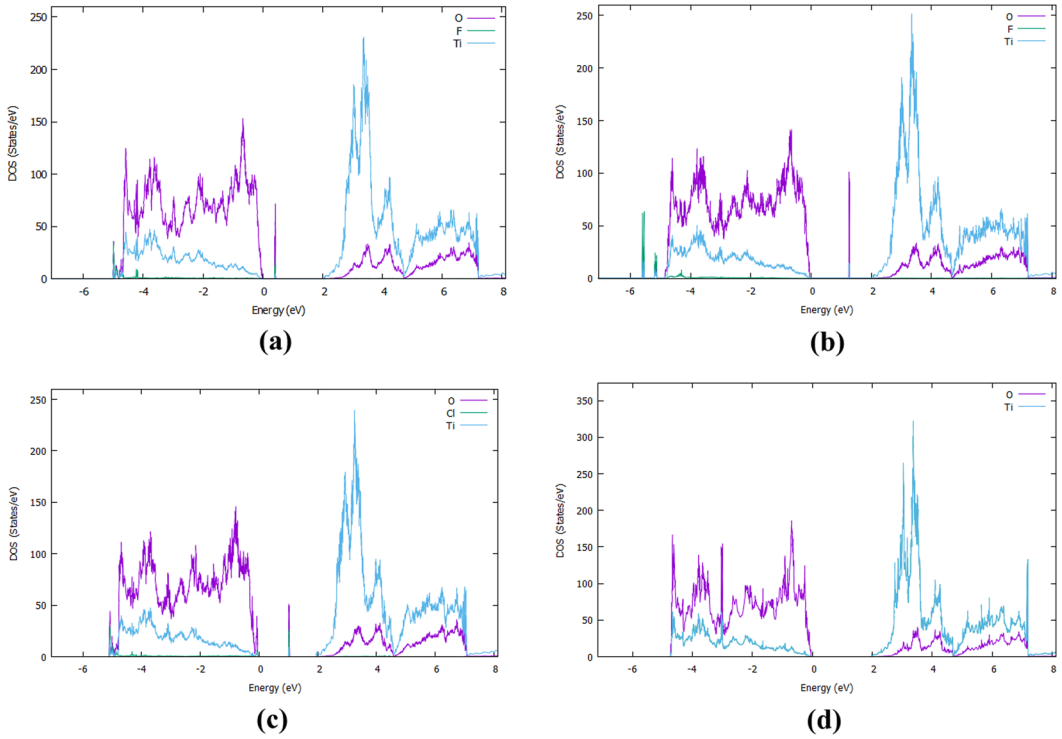

Figure 4. (**a**) The Projected DOS (PDOS) of the bulk F:TiO_2 with F an interstitial, (**b**) The Projected DOS of the bulk F:TiO_2 with F occupying an oxygen site and displaying the oxygen to an interstitial site, (**c**) The Projected DOS of the Bulk Cl:TiO_2 with Cl an interstitial, (**d**) The PDOS of TiO_2.

see that the conduction band is mainly attributed to Ti while the valence band to O. In more detail,in Fig. 5a, it is shown that the main contributions to the valence and the conduction bands are attributed mainly to the O-2p and Ti-3d respectively. As far as the rise of mid-gap states (Fig. 5b) is concerned, we found that it is mainly attributed to the O-2p and F-2p orbitals. Concerning the minimum energy configuration with a fluorine replacing an oxygen which is displaced to an interstitial, two mid-gap levels emerge, one at 0.48 eV and one at 2.02 eV above the VB maximum. Moreover, it is seen that the band gap decreases by approximately 0.10 eV, reaching a value of 3.04 eV. To shed more light on these mid-gap peaks, a PDOS calculation was conducted again and presented in Fig. 4b. As one can see in Fig. 5d, the main contributions to these mid-gap levels come from O-2p and Ti-3d with and only a minimal contribution originates from fluorine, unlike the previous case of the F interstitial (Fig. 5b). A similar DFT research was conducted by Valentin and Pacchioni[45] and they calculated that when F is inserted as a substitutional defect, the band gap is reduced to 3.08 eV which is also in a good agreement with the present results. Samsudin and Hamid[46] have done an important experimental work on the band gap engineering of anion doped TiO_2 and they calculated that the band gap of TiO_2 is significantly decreased to 3.02 eV, which is again consistent with the present DFT work.

For the bulk Cl:TiO_2, in the case of a Cl interstitial, the DOS (Fig. 3d) shows peaks at 0.19 eV and 1.38 eV above the conduction band minimum and, in addition, the band gap of the bulk TiO_2 is significantly reduced to 2.89 eV. Looking at the PDOS of the bulk with Cl interstitial, we see that the valence and the conduction bands mainly consist of Ti-3d and O-2p and the mid-gap peak of O-2p and Cl-2p states. For the case of Cl substituting an O, one can see that a mid-gap peak appears again, at 1.77 eV, while the band gap is reduced to 2.84 eV (Figs. 1d and 2f). Focusing on the experimental work of Sun *et al.*[47] it is seen that the band gap of the Cl:TiO_2 reaches a value of 2.98 eV. This experimental work is also in agreement with our calculations, therefore it is suggested that band gap engineering of TiO_2 can be used to a number of applications such as photocatalysis.

Surface of anatase TiO_2. In order to develop better photocatalytic materials with visible light response and high activity, such as TiO_2, more attention should be paid to surface doping with atoms or molecules. However, theoretical investigations of the effect of the surface doping on the surface electronic structure of TiO_2 are at present scarce compared to the studies concerning the bulk system[48]. The aim of this section is to investigate the structural and electronic properties of the F- and Cl- doped TiO_2 surface by using a DFT + U, in spin polarized calculations. We calculated the interatomic distances and angles, the electronic density of states of the undoped and doped TiO_2 surface, as well as the changes of the band gap when the system is doped. For the simulation of the surfacewe used a slab model with a vacuum of 14 Å thickness vertical to the (001) plane and with periodic boundary conditions in the other directions. In our surface system, the top 4 layers were fully relaxed while the bottom 4 layers were kept fixed in order to simulate the bulk area. We chose this particular surface because it is a common choice in other studies concerning the absorption of different atoms and molecules, like CO_2[49], but the

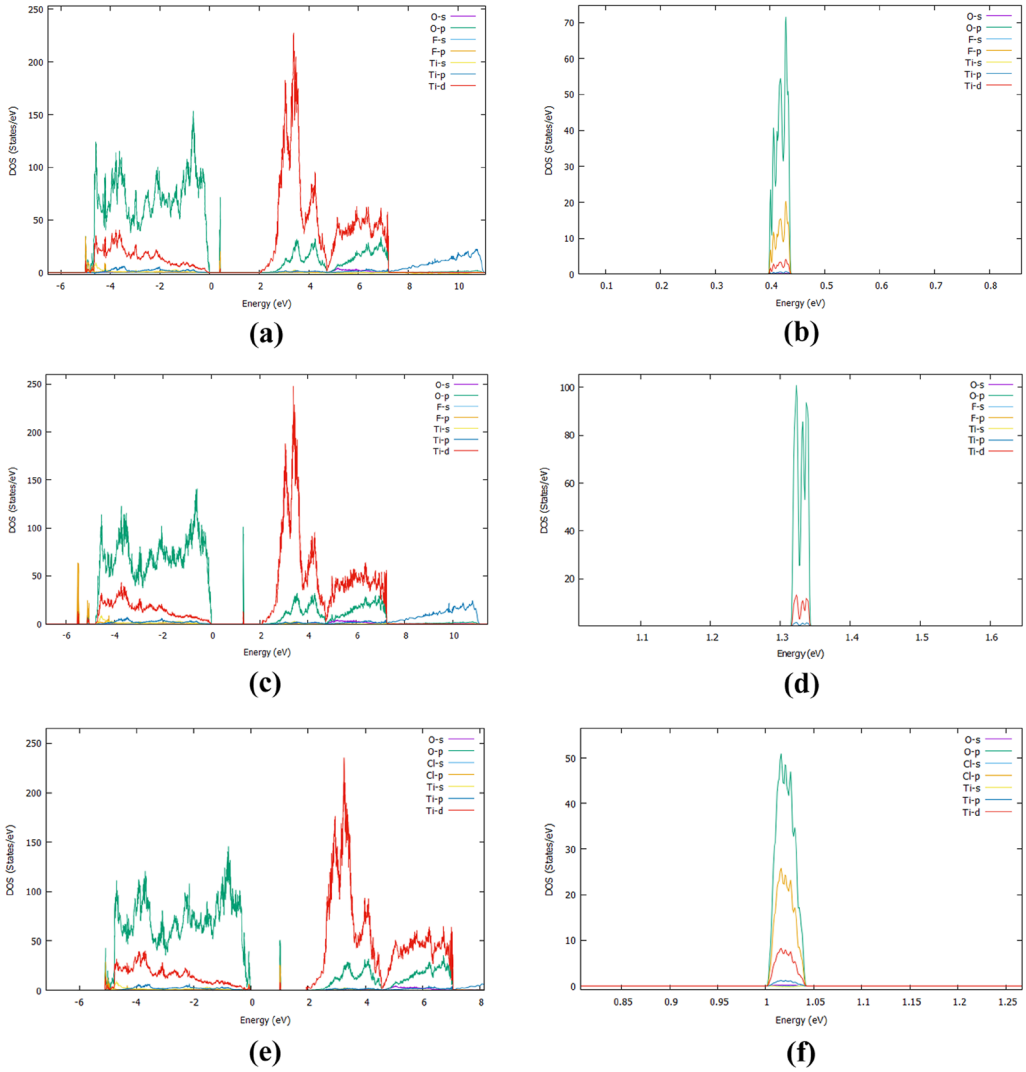

Figure 5. (**a**) The PDOS coming from the orbitals for the bulk F:TiO_2, (**b**) The orbitals contribution to the mid gap rise of the bulk F:TiO_2, (**c**) The PDOS from the orbitals of F:TiO_2 when F occupies an oxygen position and displaces the oxygen to an interstitial site, (**d**) the orbitals contribution to the mid gap rise of F:TiO_2 when F occupies an oxygen site and displaces oxygen to an interstitial, (**e**) The PDOS coming from the orbitals for the bulk Cl:TiO_2, (**f**) The orbitals contribution to the mid gap rise of the bulk Cl:TiO_2.

interstitial-doping with fluorine or chlorine atoms has never been studied before. Instead, the (101) surface has mostly been considered for fluorine and chlorine doping[50]. However, the (001) TiO_2 surface is considered one of the most highly energetic surfaces of the TiO_2 and, as a result, it often plays the role of the active site in photocatalytic reactions[51–55]. To the best of our knowledge only Zhou p. *et al.*[56] have studied the TiO_2 (001) surface in the case of F doping as a substitution of an O atom. The undoped configuration is shown in Fig. 6a while the minimum energy structures for F and Cl doped TiO_2 (001) surfaces are shown in Fig. 6b,c respectively.

According to our DFT calculations, when fluorine is inserted in the (001) surface as an interstitial (Fig. 7a), it is located at a distance of 2.00 Å from the nearest oxygen while Cl (Fig. 7b) at 2.18 Å. Looking at the DOS for each supercell, in Fig. 8a it is seen that the F interstitial at the surface produces a small impurity band peak at approximately 0.35 eV above the VB. On the other hand, as it is seen in Fig. 8b, when the surface is doped with a Cl atom, two mid-gap peaks arise, which are observed at approx. 0.55 eV and 0.93 eV above the valence band. Concerning the band gap, when the TiO_2 surface is doped with F, the band gap is predicted at a value of 2.24 eV whereas for the Cl–doped surface, the calculated band gap reaches a value of 2.31 eV. The band gap of the undoped TiO_2 surface calculated at 2.37 eV(Fig. 8c) in agreement with other theoretical studies concerning (001) TiO_2 surfaces[57]. Therefore, the insertion of F or Cl on the (001) surface, has a minor effect on the band gap of the TiO_2 system.

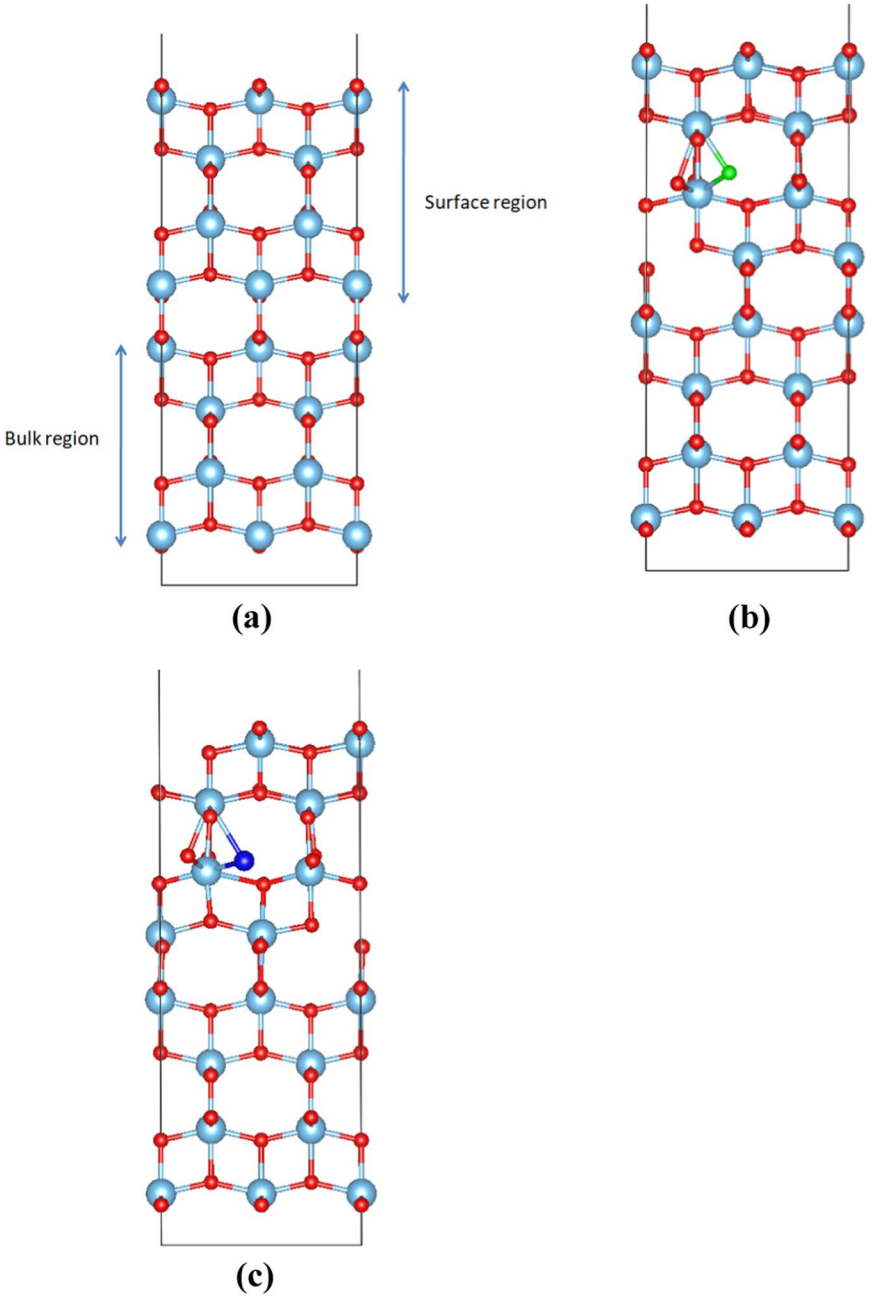

Figure 6. (**a**) The model for the TiO_2 (001) surface where the bottom 4 layers represent the bulk region and the top 4 layers the surface region, (**b**) The F doped TiO_2 (001) surface, (**c**) The Cl doped TiO_2 (001) surface.

Conclusions

DFT calculations were performed for fluorine and chlorine-doped anatase TiO_2 bulk and surface structures in order to evaluate the effect this kind of doping on the band gap and the electronic structure of TiO_2. Both substitutional and interstitial halogen defects were predicted. In all cases, occupied mid-gap states attributed to a hybridization of O-2p with halogen 1 s orbitals were also predicted. Although such states are beneficial for the oxide's photocatalytic activity as they significantly reduce the optical band gap with respect to that of undoped TiO_2, they might be detrimental for its application as electron transport material in other classes of photovoltaic devices such as organic and perovskite solar cells.

Methods

Computational methodology. We performed periodic DFT calculations using the CASTEP program[58,59]. The Perdew, Burke and Ernzerhof (PBE)[60] generalized gradient approximation (GGA) functional was employed for the exchange and correlation interactions with ultrasoftpseudopotentials[61]. The cut-off Energy was chosen at 480 eV and a $3 \times 3 \times 1$ Monkhorst-Pack (MP)[62] k-points mesh while supercells of 108 atoms were adopted for

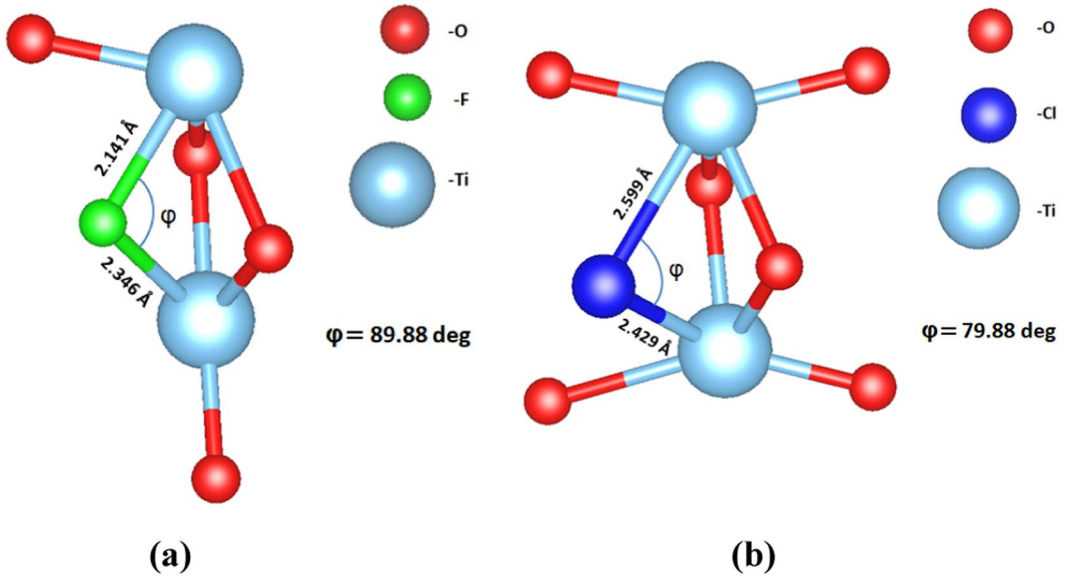

Figure 7. (**a**) Fluorine interstitial in the (001) TiO_2 surface, (**b**) Chlorine interstitial in the (001) TiO_2 surface.

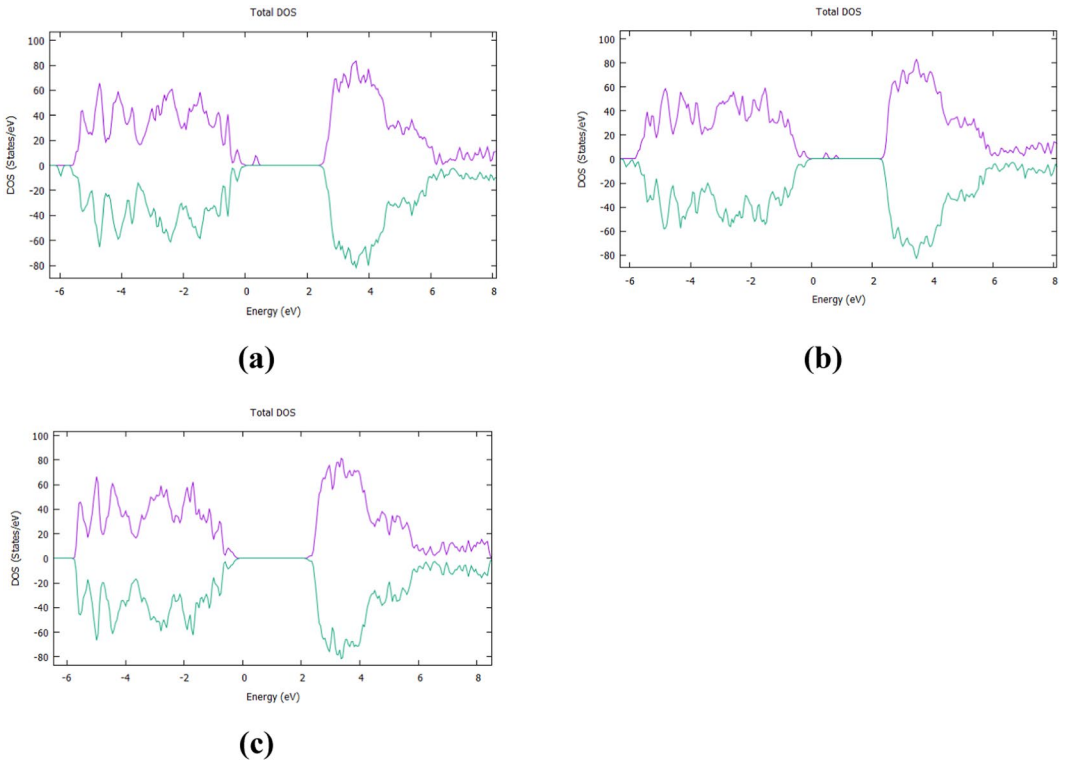

Figure 8. (**a**) DOS of F-doped TiO_2 (001) surface with F an interstitial, (**b**) DOS of Cl:TiO_2 (001) surface when Cl is an interstitial. (**c**) DOS of (001) surface of anatase TiO_2.

the bulk system.The structure was optimized with the Broyden-Fletcher-Goldfarb-Shanno (BFGS) method. To consider the effects of electronlocalization, the DFT + U method was employed for spin-polarized calculations with on-site Coulomb repulsions of 8.2 eV for the 3d orbitals of Ti. Finally, for the DOS calculations, a $3 \times 3 \times 3$ k-points mesh of was adopted while for the PDOS a $7 \times 7 \times 7$. The efficacy of the present approach has been demonstrated in recent studies[10,11]. For the surface structures, a supercell consisting of 96 atoms was used, with an energy cut off of 480 eV and a MP k-point mesh of $2 \times 2 \times 1$. Finally, for the density of states, we chose a $7 \times 7 \times 7$ k-point mesh.

Received: 9 October 2019; Accepted: 11 November 2019;
Published online: 27 December 2019

References

1. Fujishima, A. & Honda, K. Electrochemical photolysis of water at a semiconductor electrode. *Nature* **238**, 5358 (1972).
2. Gratzel, M. Photoelectrochemical cells. *Nature* **414**, 338–344 (2001).
3. Asahi, R., Morikawa, T., Ohwaki, T., Aoki, K. & Taga, Y. Visible-light photocatalysis in nitrogen-doped titanium oxides. *Science* **293**, 269–271 (2001).
4. Khan, S. U. M., Al-Shahry, M. & Ingler, W. B. Efficient photochemical water splitting by a chemically modified n-TiO_2. *Science* **297**, 2243–2245 (2002).
5. Russo, S. P., Grey, I. E. & Wilson, N. C. Nitrogen/hydrogen codoping of anatase: A DFT study. *J. Phys. Chem. C* **112**, 7653–7664 (2008).
6. Yang, H. G. *et al*. Anatase TiO_2 single crystals with a large percentage of reactive facets. *Nature* **453**, 638–641 (2008).
7. Gai, Y., Li, J., Li, S.-S., Xia, J.-B. & Wei, S.-H. Design of narrow-gap TiO_2: A passivated codoping approach for enhanced photoelectrochemical activity. *Phys. Rev. Lett.* **102**, 036402 (2009).
8. Dou, L. *et al*. Tandem Polymer Solar Cells Featuring a Spectrally Matched Low-Bandgap Polymer. *Nat. Photonics* **6**, 180–185 (2012).
9. Sivula, K. & van de Krol, R. Semiconducting materials for photoelectrochemical energy conversion. *Nat. Mater. Rev.* **1**, 15010 (2016).
10. Zhu, J. *et al*. Intrinsic defects and H doping in WO3. *Sci. Rep.* **7**, 40882 (2017).
11. Qiu, Y., Chen, W. & Yang, S. Double-layered photoanodes from variable-size anatase TiO_2 nanospindles: a candidate for high-efficiency dye-sensitized solar cells. *AngewandteChemie International Edition* **49**(21), 3675–3679 (2010).
12. Ullattil, S. G. *et al*. Sol-solvothermal processed 'black TiO_2 asphotoanode material in dye sensitized solar cells. *Sol. Energy* **155**, 490–495 (2017).
13. Govindaraj, R., Santhosh, N., Pandian, M. S., Ramasamy, P. & Sumita, M. Fabrication of stable dye-sensitized solar cell with hydrothermally synthesized titanium dioxide nanorods as a photoanode material. *J. Mater. Sci. Mater. Electron.* **29**, 3736–3743 (2018).
14. Sauvage, F. *et al*. Hierarchical, TiO_2 photoanode for dye-sensitized solar cells. *Nano Lett.* **10**(7), 2562–2567 (2010).
15. Zhu, K., Neale, N. R., Miedaner, A. & Frank, A. J. Enhanced charge-collection efficiencies and light scattering in dye-sensitized solar cells using oriented TiO_2 nanotubes arrays. *Nano Lett.* **7**(1), 69–74 (2007).
16. Mor, G. K., Shankar, K., Paulose, M., Varghese, O. K. & Grimes, C. A. Use of highly-ordered TiO_2 nanotube arrays in dye-sensitized solar cells. *Nano Let.* **6**(2), 215–218 (2006).
17. Wang, Z. *et al*. Enhanced performance of perovskite solar cells by ultraviolet-ozone treatment of mesoporous TiO_2. *Appl. Surf. Sci.* **436**, 596–602 (2018).
18. Zhang, D., Xie, F., Lin, P. & Choy, W. C. Al-TiO_2 composite-modified single-layer graphene as an efficient transparent cathode for organic solar cells. *ACS Nano* **7**(2), 1740–1747 (2013).
19. Seo, H. O. *et al*. Ultrathin TiO_2 films on ZnO electron-collecting layers of inverted organic solar cell. *J. Phys. Chem.* **C115**(43), 21517–21520 (2011).
20. Zhang, D. *et al*. Plasmonic electrically functionalized TiO_2 for high-performance organic solar cells. *Adv. Funct. Mater.* **23**(34), 4255–4261 (2013).
21. Lira-Cantu, M., Chafiq, A., Faissat, J., Gonzalez-Valls, I. & Yu, Y. Oxide/polymer interfaces for hybrid and organic solar cells: Anatase vs. Rutile TiO_2. *Sol. Energ. Mat. Sol. Cells* **95**(5), 1362–1374 (2011).
22. Lin, Z., Jiang, C., Zhu, C. & Zhang, J. Development of inverted organic solar cells with TiO_2 interface layer by using low-temperature atomic layer deposition. *ACS Appl. Mater. Interfaces* **5**(3), 713–718 (2013).
23. Green, M. A., Ho-Baillie, A. & Snaith, H. J. The emergence of perovskite solar cells. *Nat. Photonics* **8**(7), 506–514 (2014).
24. Kim, H. S. & Park, N. G. Parameters affecting I–V hysteresis of CH3NH3PbI3perovskite solar cells: effects of perovskite crystal size and mesoporous TiO_2 layer. *J. Phys. ChemLett.* **5**(17), 2927–2934 (2014).
25. Pathak, S. K. *et al*. Performance and stability enhancement of dye-sensitized and perovskite solar cells by Al doping of TiO_2. *Adv. Funct. Mater.* **24**(38), 6046–6055 (2014).
26. Serpone, N. Is the Band Gap of Pristine TiO_2 Narrowed by Anion- and Cation-Doping of Titanium Dioxide in Second-Generation Photocatalysts? *J. Phys. Chem. B* **110**, 24287–24293 (2006).
27. Vasilopoulou, M. *et al*. Hydrogen and nitrogen codoping of anatase TiO_2 for efficiency enhancement in organic solar cells. *Sci. Rep.* **7**(1), 17839 (2017).
28. Wang, J. *et al*. Origin of photocatalytic activity of nitrogen-doped TiO_2 nanobelts. *J. Am. Chem. Soc.* **131**(34), 12290–12297 (2009).
29. Czoska, A. *et al*. The nature of defects in fluorine-doped TiO_2. *J. Phys. Chem.* **C112**(24), 8951–8956 (2008).
30. Zhao, Y. *et al*. Zn-doped TiO_2 nanoparticles with high photocatalytic activity synthesized by hydrogen–oxygen diffusion flame. *Appl. Catal. B Environ.* **79**(3), 208–215 (2008).
31. Yang, K., Dai, Y., Huang, B. & Whangbo, M. H. Density functional characterization of the band edges, the band gap states, and the preferred doping sites of halogen-doped TiO_2. *Chem. Mater.* **20**(20), 6528–6534 (2008).
32. Sharma, S. D. *et al*. Sol–gel-derived super-hydrophilic nickel doped TiO_2 film as active photo-catalyst. *Appl. Catal. A Gen.* **314**(1), 40–46 (2006).
33. Kordatos, A., Kelaidis, N. & Chroneos, A. Defect pair formation in fluorine and nitrogen codoped TiO_2. *J. Appl. Phys.* **123**(16), 161510 (2018).
34. Kelaidis, N., Kordatos, A., Christopoulos, S.-R. G. & Chroneos, A. A roadmap of strain in doped anatase TiO_2. *Sci. Rep.* **8**, 12790 (2018).
35. Pan, X., Yang, M. Q., Fu, X., Zhang, N. & Xu, Y. J. Defective TiO_2 with oxygen vacancies: synthesis, properties and photocatalytic applications. *Nanoscale* **5**, 3601–3614 (2013).
36. Pan, X., Yang, M.-Q. & Xu, Y.-J. Morphology control, defect engineering andphotoactivity tuning of ZnO crystals by grapheneoxide–a unique 2D macromolecular surfactant. *Phys. Chem. Chem. Phys.* **16**, 5589–5599 (2014).
37. Babu, V. J., Nair, A. S., Peining, Z. & Ramakrishna, S. Synthesis and characterization of rice grains like Nitrogen-doped TiO_2 nanostructures by electrospinning–photocatalysis. *Mater.Lett.* **65**(19-20), 3064–3068 (2011).
38. Khan, S. *et al*. Defect engineering toward strong photocatalysis of Nb-doped anatase TiO_2: Computational predictions and experimental verifications. *Appl. Catal.* **B206**, 520–530 (2017).
39. Lin, Y. *et al*. The electronic structure, optical absorption and photocatalytic water splitting of (Fe+ Ni)-codoped TiO_2: A DFT+ U study. *Int. J. Hydrogen Energy* **42**(8), 4966–4976 (2017).
40. Di Valentin, C. & Pacchioni, G. Trends in non-metal doping of anatase TiO_2: B, C, N and F. *Cat. today* **206**, 12–18 (2013).
41. Samsudin, E. M. & Hamid, S. B. A. Effect of band gap engineering in anionic-doped TiO_2 photocatalyst. *Appl. Surf. Sci.* **391**, 326–336 (2017).
42. Sun, H., Wang, S., Ang, H. M., Tadé, M. O. & Li, Q. Halogen element modified titanium dioxide for visible light photocatalysis. *Chem. Eng. J.* **162**(2), 437–447 (2010).
43. Nagpal, P. & Klimov, V. I. Role of mid-gap states in charge transport and photoconductivity in semiconductor nanocrystal films. *Nature Commun.* **2**, 486 (2011).

44. Luttrell, T. *et al*. Why is anatase a better photocatalyst than rutile?-Model studies on epitaxial TiO_2 films. *Sci. Rep.* **4**, 4043 (2014).
45. Burdett, J. K., Hughbanks, T., Miller, G. J., Richardson, J. W. Jr. & Smith, J. V. Structural-electronic relationships in inorganic solids: powder neutron diffraction studies of the rutile and anatase polymorphs of titanium dioxide at 15 and 295 K. *J. Am. Chem. Soc.* **109**(12), 3639–3646 (1987).
46. Muscat, J., Swamy, V. & Harrison, N. M. First-principles calculations of the phase stability of TiO_2. *Phys. Rev.* **B65**(22), 224112 (2002).
47. Tosoni, S., Lamiel-Garcia, O., Fernandez Hevia, D., Doña, J. M. & Illas, F. Electronic structure of F-doped bulk rutile, anatase, and brookite polymorphs of TiO_2. *J. Phys. Chem.* **C116**(23), 12738–12746 (2012).
48. Araujo-Lopez, E., Varilla, L. A., Seriani, N. & Montoya, J. A. TiO_2 anatase's bulk and (001) surface, structural and electronic properties: a DFT study on the importance of Hubbard and van der Waals contributions. *Surf. Sci.* **653**, 187–196 (2016).
49. Zhao, Z., Li, Z. & Zou, Z. First-Principles Calculations on Electronic Structures of N/V-Doped and N-V- DodopedAnatase TiO_2 (101) Surfaces. *Chem. Phys. Chem.* **13**(17), 3836–3847 (2012).
50. Lazzeri, M., Vittadini, A. & Selloni, A. Structure and energetics of stoichiometric TiO_2 anatase surfaces. *Phys. Rev. B* **63**(15), 155409 (2001).
51. Liu, S., Yu, J. & Jaroniec, M. Anatase TiO_2 with dominant high-energy {001} facets: synthesis, properties, and applications. *Chem. Mater.* **23**(18), 4085–4093 (2011).
52. Wang, X., He, H., Chen, Y., Zhao, J. & Zhang, X. Anatase TiO_2 hollow microspheres with exposed {001} facets: Facile synthesis and enhanced photocatalysis. *Appl. Surf. Sci.* **258**(15), 5863–5868 (2012).
53. Liu, M., Li, H., Zeng, Y. & Huang, T. Anatase TiO_2 single crystals with dominant {001} facets: Facile fabrication from Ti powders and enhanced photocatalytical activity. *Appl. Surf. Sci.* **274**, 117–123 (2013).
54. Gu, L., Wang, J., Zou, Z. & Han, X. Graphitic-C3N4-hybridized TiO_2 nanosheets with reactive {001} facets to enhance the UV-and visible-light photocatalytic activity. *J. Hazard. Mater.* **268**, 216–223 (2014).
55. Long, J. *et al*. 2014. Gold-plasmon enhanced solar-to-hydrogen conversion on the {001} facets of anatase TiO_2 nanosheets. *Energy Environ. Sci.* **7**(3), 973–977 (2014).
56. Zhou, P. *et al*. Vectorial doping-promoting charge transfer in anatase TiO_2 {0 0 1} surface. *Appl. Surf. Sci.* **319**, 167–172 (2014).
57. Li, H., Guo, Y. & Robertson, J. Calculation of TiO_2 surface and subsurface oxygen vacancy by the screened exchange functional. *J. Phys. Chem.* **C119**(32), 18160–18166 (2015).
58. Payne, M. C., Teter, M. P., Allan, D. C., Arias, T. A. & Joannopoulos, J. D. CASTEP 4.2 Academic version, licensed under the UKCP-MSI Agreement. *Rev. Mod. Phys.* **64**, 1045–1097 (1992).
59. Segall, M. D. *et al*. First-principles simulation: ideas, illustrations and the CASTEP code. *J. Phys. Cond. Matter* **14**(11), 2717–2744 (2002).
60. Perdew, J. P., Burke, K. & Ernzerhof, M. Generalized gradient approximation made simple. *Phys. Rev. Lett.* **77**(18), 3865–3868 (1996).
61. Vanderbilt, D. Soft self-consistent pseudopotentials in a generalized eigenvalue formalism. *Phys. Rev.* **B41**(11), 7892–7895 (1990).
62. Monkhorst, H. J. & Pack, J. D. Special points for Brillouin-zone integrations. *Phys. Rev.* **B13**(12), 5188–5192 (1976).

Acknowledgements

P.P.F., M.V., D.D. and A.C. are grateful for LRF ICON funding from the Lloyd's Register Foundation, a charitable foundation helping to protect life and property by supporting engineering-related education, public engagement and the application of research. N.K. and N.N.L. acknowledge support by the projects "Advanced Materials and Devices" (MIS 5002409) and "National Infrastructure in Nanotechnology, Advanced Materials and Micro - / Nanoelectronics" (MIS 5002772), funded by the Operational Programme "Competitiveness, Entrepreneurship and Innovation" (NSRF 2014–2020), co-financed by Greece and the European Union (European Regional Development Fund).

Author contributions

P.P.F. and N.K. performed the calculations. P.P.F., N.K., M.V., D.D., N.N.L. and A.C. contributed to the interpretation of the results and the writing of the paper.

Competing interests

The authors declare no competing interests.

Additional information

Correspondence and requests for materials should be addressed to M.V. or A.C.

Reprints and permissions information is available at www.nature.com/reprints.

Publisher's note Springer Nature remains neutral with regard to jurisdictional claims in published maps and institutional affiliations.

Open Access This article is licensed under a Creative Commons Attribution 4.0 International License, which permits use, sharing, adaptation, distribution and reproduction in any medium or format, as long as you give appropriate credit to the original author(s) and the source, provide a link to the Creative Commons license, and indicate if changes were made. The images or other third party material in this article are included in the article's Creative Commons license, unless indicated otherwise in a credit line to the material. If material is not included in the article's Creative Commons license and your intended use is not permitted by statutory regulation or exceeds the permitted use, you will need to obtain permission directly from the copyright holder. To view a copy of this license, visit http://creativecommons.org/licenses/by/4.0/.

© The Author(s) 2019